Check for updates

Geophysical Research Letters

RESEARCH LETTER
10.1029/2025GL117015

Responses to Lower-Tropospheric Stability Dominate Intermodel Differences in the Historical Pattern Effect

Koh Kawaguchi[1,2] **and Paulo Ceppi**[1]

[1]Department of Physics, Imperial College London, London, UK, [2]Grantham Institute for Climate Change and the Environment, Imperial College London, London, UK

Key Points:

- There are large differences between models in the strength of the historical pattern effect
- These differences can be explained by different cloud radiative sensitivities to changes in lower-tropospheric stability
- Models tend to underestimate the historical time-dependence of low-cloud feedback

Supporting Information:

Supporting Information may be found in the online version of this article.

Correspondence to:

K. Kawaguchi,
k.kawaguchi24@imperial.ac.uk

Citation:

Kawaguchi, K., & Ceppi, P. (2025). Responses to lower-tropospheric stability dominate intermodel differences in the historical pattern effect. *Geophysical Research Letters*, *52*, e2025GL117015. https://doi.org/10.1029/2025GL117015

Received 12 MAY 2025
Accepted 17 AUG 2025

Abstract The sea surface temperature (SST) pattern modulates the Earth's radiative feedbacks at decadal timescales. However, decadal feedback variations over the historical period depend on the choice of climate model, even when forced with the same SST data set. We investigate these differences through analyzing amip-piForcing output, focusing on low cloud feedback. Time-variation in low cloud feedback results primarily from the SST pattern, mediated by changes in near-global lower tropospheric stability (LTS). We investigate the meteorological factors contributing to low cloud feedback variation through the cloud controlling factor analysis method, diagnosing cloud radiative sensitivities from 16 CMIP5 and CMIP6 models, and an observational constraint from MODIS. We find the radiative sensitivity of models to LTS in the stratocumulus regions dominates the magnitude of cloud feedback time variation due to the pattern effect. Additionally, models underestimate low cloud radiative sensitivity to changes in LTS and SST and thus the time-variation in feedback.

Plain Language Summary Across the historical period, the strength of Earth's feedbacks (the tendency to dampen or amplify climate responses to external forcings) has varied at decadal timescales. We examine how the latest generations of climate models represent these variations when driven by observed sea surface temperatures (SSTs). In line with existing literature, we find that the variations are driven by the evolving patterns of SST. We focus on the time-variation of the low cloud feedback, a key driver of uncertainty across models. Applying a statistical method that utilizes co-variations of clouds with the surrounding meteorology, we find that the evolving pattern of SST changes the prevalence of low cloud globally. Of the various meteorological drivers, lower-tropospheric stability (the ratio of warming at the surface and aloft) has the largest impact on model spread in the radiative response of low clouds to SST patterns. Models tend to systematically underestimate the time-variation in low cloud feedbacks because most models are not sensitive enough to lower-tropospheric stability, and all models are not sensitive enough to local changes in the SST.

1. Introduction

The Earth's global energy budget following an external forcing can be expressed through the top-of-atmosphere (TOA) energy imbalance equation $N = F + R$, where N is the energy imbalance, F the effective radiative forcing and R Earth's radiative response (Sherwood et al., 2015). The response R has traditionally been expressed as $R = \lambda \Delta T$, with λ the climate feedback parameter and ΔT the global mean surface temperature change (Gregory et al., 2004). Uncertainty in the climate feedback is dominated by the strength of cloud feedbacks, particularly from marine low clouds (Bony & Dufresne, 2005; Ceppi et al., 2017; Sherwood et al., 2020).

It is known that the climate feedback varies on decadal timescales (Figure 1a) (Gregory & Andrews, 2016; Zhou et al., 2016). This variation is caused by evolving radiative feedbacks resulting from the evolution of patterns of sea surface temperature (SST) (Figure 1b) (Andrews et al., 2015; Gregory et al., 2020; Haugstad et al., 2017). In particular, these variations are dominated by changes in the strength of low-cloud feedbacks (Figure 1c) (Andrews et al., 2015; Chao et al., 2022; Zhou et al., 2016). This dependence of radiative feedbacks on the distribution of SST has been termed the "SST pattern effect" (Stevens et al., 2016).

While numerous papers have examined the physical cause of the pattern effect (Andrews & Webb, 2018; Ceppi & Gregory, 2017; Dong et al., 2019; Williams et al., 2023; Zhou et al., 2016), relatively few studies have considered the causes of inter-model spread in its representation. Dong et al. (2020) analyzed CMIP5 and 6 models with abrupt 4 × CO_2 increases and found that the cloud feedback dominates the intermodel spread in the change in the climate feedback parameter λ across the early (1–20 years) and late (21–150 years) time periods. He et al. (2021)

© 2025. The Author(s).
This is an open access article under the terms of the Creative Commons Attribution License, which permits use, distribution and reproduction in any medium, provided the original work is properly cited.

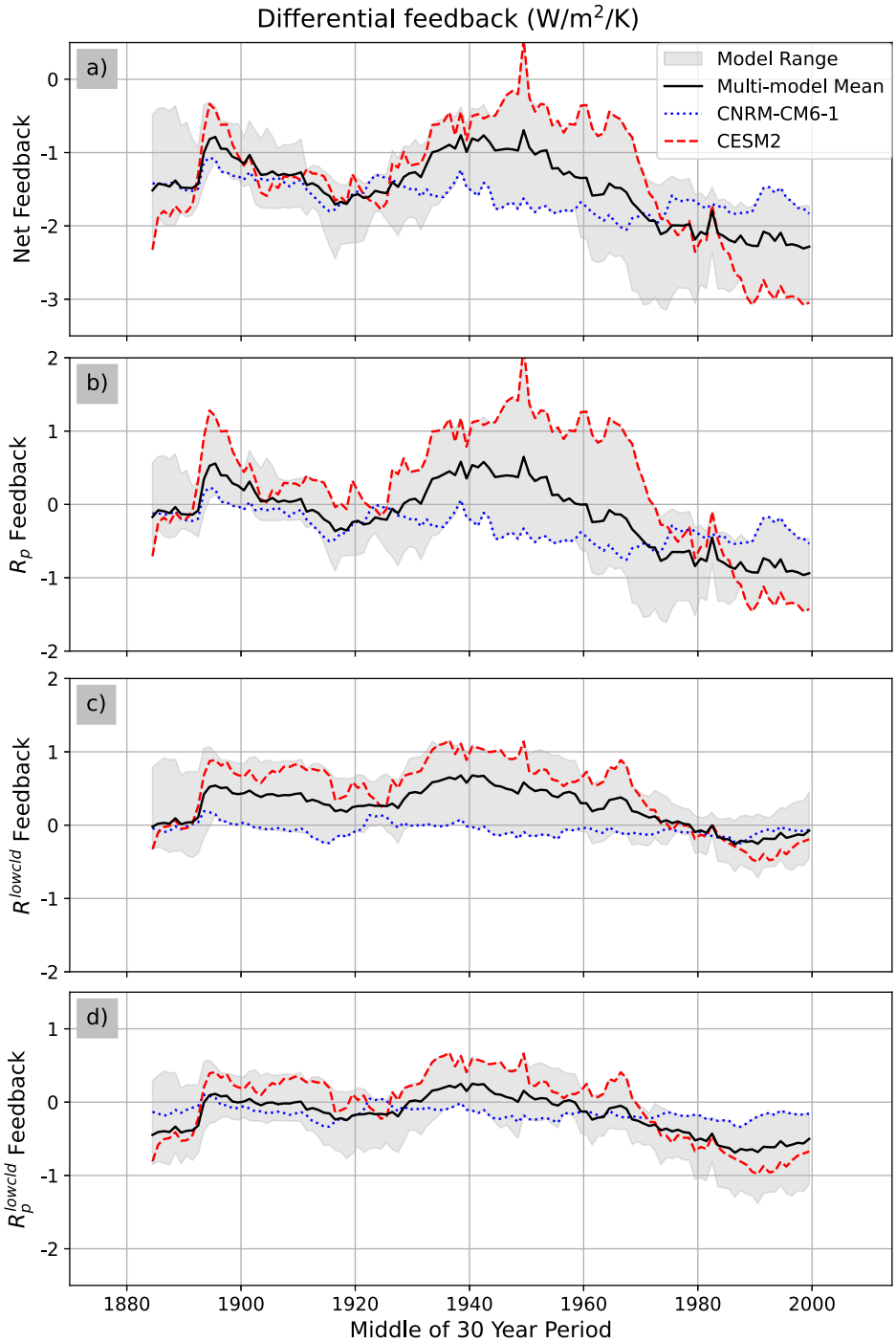


Figure 1. (a) The time-evolution of the differential climate feedback parameter for 6 models with the *amip-piForcing* experiment. The black line shows the multi-model mean, the gray shading shows the model range, the dotted blue line shows CNRM-CM6-1 and the dashed red line shows CESM2. All feedbacks have been calculated with 30-year sliding windows. (b) The same, but the time-evolution of the feedback parameter due to the pattern effect. (c) The same, but the time-evolution of the low cloud feedback. (d) The same, but the time-evolution of the low cloud feedback due to the pattern effect. See Section 2.2 for an explanation of the decomposition of the feedbacks into uniform warming and pattern components.

similarly find that variations in cloud feedbacks are dominant, but also highlight changes to relative humidity in changing lapse rate and water vapor feedbacks. Eiselt and Graversen (2022) find that in CMIP5 and 6 models without strong cloud feedbacks, changes in the lapse rate may be key in changing λ in the early and late periods

19448007, 2025, 17, Downloaded from https://agupubs.onlinelibrary.wiley.com/doi/10.1029/2025GL117015 by Imperial College London, Wiley Online Library on [30/10/2026]. See the Terms and Conditions (https://onlinelibrary.wiley.com/terms-and-conditions) on Wiley Online Library for rules of use; OA articles are governed by the applicable Creative Commons License

19448007, 2025, 17, Downloaded from https://agupubs.onlinelibrary.wiley.com/doi/10.1029/2025GL117015 by Imperial College London, Wiley Online Library on [30/10/2026]. See the Terms and Conditions (https://onlinelibrary.wiley.com/terms-and-conditions) on Wiley Online Library for rules of use; OA articles are governed by the applicable Creative Commons License

under an abrupt 4 × CO_2 experiment. However, these studies examined long-term feedback changes from coupled atmosphere-ocean models. In order to evaluate the inter-model spread due to the atmosphere, we examine the *historical pattern effect*, which we define here as the decadal variability of the climate feedback arising from observed SST variations. Note that this is distinct from the standard definition of the pattern effect which compares the difference between historical and long-term feedbacks.

The studies that do evaluate the historical pattern effect find a diverse range of model responses but do not tend to focus on the reason for intermodel variation (Andrews et al., 2018, 2022; Silvers et al., 2018). Marvel et al. (2018) find that model sensitivity of low cloud cover to SST may explain the model spread in feedback estimates from 27 years of data, but do not examine time-variations. In this paper, we provide the first comprehensive examination of intermodel spread in the SST pattern response and focus in particular on low cloud feedbacks resulting from the SST pattern effect as a cause of intermodel spread.

2. Data and Methods

2.1. Summary of CG19 Framework

We follow the framework of Ceppi and Gregory (2019, hereafter CG19), where the radiative response R is decomposed into a component associated with spatially uniform changes in global-mean temperature, R_{unif}, and another associated with changes in the SST pattern, R_p. In particular, the radiative response can be modeled as

$$R = R_{\text{unif}} + R_p = \tau \Delta T + \sigma \Delta S_p. \tag{1}$$

ΔS is the change in near-global estimated inversion strength (EIS) (defined over the ocean equatorward of 50° latitude), and ΔS_p is the component of ΔS induced by the SST pattern (where changes in S due to uniform warming have been removed) (Wood & Bretherton, 2006). τ and σ are the feedback parameters to ΔT and ΔS_p respectively. The relationship between the traditional feedback parameter λ and τ, σ is obtained by differentiating Equation 1 with respect to T:

$$\lambda = \frac{dR}{dT} = \tau + \sigma \frac{dS_p}{dT}. \tag{2}$$

hence in CG19, time-variation in the strength of the feedback parameter λ is due to changes in global lower-tropospheric stability induced by the SST warming pattern.

One modification we make to CG19's framework is that we assume the uniform warming and pattern effect induces a linear response with respect to T and S_p respectively (i.e., we assume that τ, σ are constants). We make this assumption due to insufficient instances of uniform warming/cooling in existing model output to accurately determine non-linearity, although we note that the small variation in global-mean T suggests that non-linearity due to state-dependence would be small.

2.2. Uniform Warming and Pattern Effect Decomposition

We analyze output from 6 models in CMIP6, selecting all models with International Satellite Cloud Climatology Project (ISCCP) simulator output available for the experiments *amip-piForcing, amip-p4K* and *amip-m4K* (hereafter *piForcing*, *p4K* and *m4K* respectively) from the Cloud Feedback Model Intercomparison Project (CFMIP) (Bodas-Salcedo et al., 2011; Webb et al., 2017). The list of models is available in Table S1 of Supporting Information S1. *p4K* and *m4K* refer to atmosphere-only experiments driven by prescribed SSTs and sea ice in which the SST has been uniformly increased or decreased by 4K respectively, relative to the AMIP II data set between 1979 and 2014, with realistic concentrations of CO_2 and aerosols (Hurrell et al., 2008; Webb et al., 2017). We diagnose the atmospheric response to a uniform increase in SST from the *p4K* and *m4K* experiments in the following way. For each local variable $X(\vec{r})$, we estimate the change associated with a uniform surface temperature increase of 1K as the time mean of $\frac{dX(\vec{r})}{dT_{\text{unif}}}$ in the following equation:

$$\frac{dX(\vec{r})}{dT_{\text{unif}}} \approx \frac{X_{p4K}(\vec{r}) - X_{m4K}(\vec{r})}{T_{p4K} - T_{m4K}}, \tag{3}$$

19448007, 2025, 17, Downloaded from https://agupubs.onlinelibrary.wiley.com/doi/10.1029/2025GL117015 by Imperial College London, Wiley Online Library on [30/10/2026]. See the Terms and Conditions (https://onlinelibrary.wiley.com/terms-and-conditions) on Wiley Online Library for rules of use; OA articles are governed by the applicable Creative Commons License

where T_{x4K} is the mean global surface temperature for each experiment, and similarly for X. We follow the approach of Ceppi and Fueglistaler (2021) by using *p4K* and *m4K* and take centered differences, rather than calculating forward differences from the *amip* run and *p4K*, to reduce errors due to assuming linearity in uniform warming.

We determine the effect of changing historical SST patterns using *piForcing*, an atmosphere-only experiment where concentrations of all forcing agents (anthropogenic and natural) are held fixed at the pre-industrial level (hence $F = 0$ by construction), and SSTs and sea ice are taken from the AMIP II data set between 1870 and 2014. For each variable X, we firstly calculate the anomaly X_{anom} with respect to the whole *piForcing* experiment period (1870–2014), and then calculate the pattern component as

$$X_p(\vec{r}) = X_{\text{anom}}(\vec{r}) - \frac{dX(\vec{r})}{dT_{\text{unif}}} T_{\text{anom}}, \tag{4}$$

where T_{anom} is the global mean surface temperature anomaly relative to the *piForcing* experiment period. All model data was interpolated to a $5^\circ \times 5^\circ$ latitude-longitude grid and resampled to annual data.

We also investigate the low cloud response to SST patterns as it is known that marine low clouds are a key driver of model uncertainty in feedbacks in coupled atmosphere-ocean models (Bony & Dufresne, 2005; Zelinka et al., 2020), and that the variation in the climate feedback parameter across the historical period is primarily from low clouds (Andrews et al., 2022; Zhou et al., 2016). We calculate low cloud radiative anomalies for *piForcing* and the low cloud radiative response to uniform warming from *p4K/m4K* by convolving output from the ISCCP simulator with the cloud radiative kernels of Zelinka et al. (2012), following the approach of Zelinka et al. (2025). Given Ceppi et al. (2024) find that ISCCP simulator output misattributes some low clouds to the third lowest pressure bin, we define low cloud for calculating radiative anomalies as clouds which have cloud top pressure greater than 560 hPa rather than the more common 680 hPa. Owing to missing values during polar night, we only use data equatorward of 60° latitude, and scale values to the global area when taking area averages.

2.3. Time-Variation of the Feedback Parameter

We calculate the differential feedback parameter λ by regressing the net TOA radiative anomalies $N = R$ of the *piForcing* runs against T using 30-year sliding windows (Andrews et al., 2022; Gregory & Andrews, 2016; Zhou et al., 2016) (Figure 1a). As the uniform component is governed by distinct physical processes which may obscure our analysis, we also calculate the feedback associated with the pattern component of the radiative response, R_p (Figure 1b). We find that the models tend to co-vary with each other over time. Additionally, the inter-model spread is dominated by the pattern component, although there is some spread in the uniform component which appears as a constant offset (Figure 1b, Table S2 in Supporting Information S1). Note that the spread in the uniform component is purely due to model differences from Equation 3; the spread in the uniform component has already been investigated in previous studies (e.g., Ringer et al., 2014; Ringer et al., 2023).

3. Low Cloud Feedback Dominates the Inter-Model Variance in the Historical Pattern Effect

Under the CG19 framework, inter-model variation in R_p can come from three possible factors.

1. Inter-model differences in the SST pattern;
2. Different dynamical responses resulting in different S_p given the same SST pattern; and
3. Different radiative responses resulting in different R_p given the same S_p, that is, differences in σ Equation 1.

By using *piForcing*, we have controlled for the SST pattern, as all models use the same SST data set. We examine the time-series of S_p and observe that the inter-model variation in S_p is small compared to the time variation, suggesting that intermodel differences in the dynamical response to a given SST are small (Figure S1 in Supporting Information S1). Finally, we model the radiative response as $R_p = \sigma S_p$, and apply linear regression to estimate σ. We find that R_p and S_p are linearly related in all models ($r < -0.6$ in every model), with values of σ varying between -2.18 and -5.79 W/m^2/K (Figure 2a). This agrees with CG19, who found substantial inter-model differences between CAM4 and HadAM3 in the strength of the radiative response to S_p. Combining

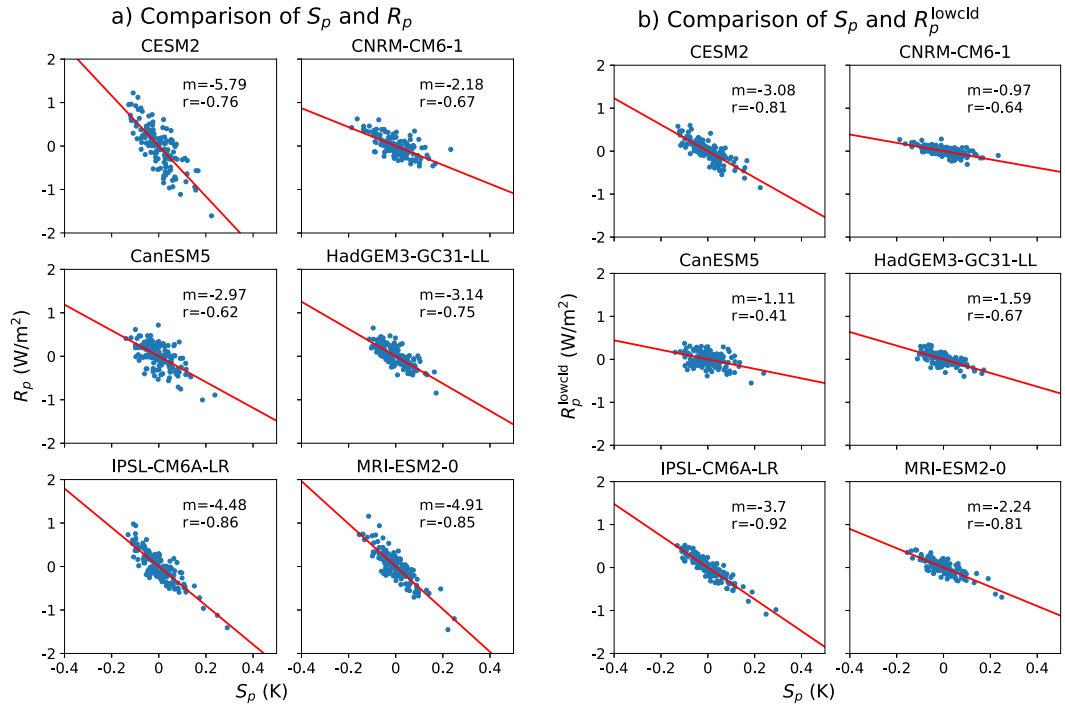


Figure 2. (a) Scatterplots of R_p versus. S_p for 6 CMIP6 models. The best fit lines are in red, with the slopes denoted by m and the correlation coefficient by r (b) The same, but for R_p^{lowcld} versus S_p.

these findings suggests that variations in R_p due to the SST pattern arise due to differences in the radiative response (factor (iii) above), rather than different large-scale dynamical responses to the SST pattern (factor (ii)). This is further supported by the fact that the CMIP6 models tend to co-vary in their R_p feedback in Figure 1b; this occurs because the S_p induced by the same SST pattern is similar across models, with the magnitude of the response varying.

We further hypothesize that the inter-model differences in the radiative response result from differences in the radiative response of the low clouds. This is because the pattern effect acts primarily through lapse rate and low cloud responses to changes in the lower tropospheric stability (LTS) (Andrews & Webb, 2018; Ceppi & Gregory, 2019; Dong et al., 2019; Zhou et al., 2017). Additionally, while the lapse rate response is linearly related to S_p, the spread is very small (Figure S2 and Text S2 in Supporting Information S1). Indeed, we find that the time-variation in the net feedback is highly correlated with the time-variation in the pattern component of the low-cloud feedback R_p^{lowcld} (Figures 1a–1d, $r = 0.94$ for the multi-model mean). We compare the low cloud radiative anomaly due to the SST pattern R_p^{lowcld} with S_p. We calculate R_p^{lowcld} for all grid-boxes with latitudes equatorward of 60°, and calculate a globally weighted low cloud sensitivity to S_p (Figure 2b). We find that R_p^{lowcld} is also linearly related to S_p and that the model sensitivities of R_p and R_p^{lowcld} to S_p are highly correlated ($r = 0.82$). Thus having shown that model differences in the overall radiative response result from differences in low clouds, we apply a sensitivity analysis and verify that most of the model spread in the time-variation of low cloud feedback results from differences in the radiative sensitivity, further solidifying our confidence that factor (iii) above is the dominant cause of model differences (Figure S3 and Text S3 in Supporting Information S1). Given that a large amount of the model sensitivity is explained by the low cloud response, in the next section we further decompose the causes of differing low cloud radiative response.

19448007, 2025, 17, Downloaded from https://agupubs.onlinelibrary.wiley.com/doi/10.1029/2025GL117015 by Imperial College London, Wiley Online Library on [30/10/2026]. See the Terms and Conditions (https://onlinelibrary.wiley.com/terms-and-conditions) on Wiley Online Library for rules of use; OA articles are governed by the applicable Creative Commons License

4. Explaining Low Cloud Feedbacks With CCF Analysis

4.1. Framework

We decompose the differing low cloud radiative responses between models by applying cloud controlling factor (CCF) analysis. The method is based on the observation that low clouds respond to regional meteorological variables (the CCFs) on monthly timescales (Klein et al., 2017; Stevens & Brenguier, 2009). The radiative response of clouds to changes in the meteorology can be estimated as a first-order Taylor expansion of the cloud radiative response to changes in the CCFs as follows:

$$\Delta R^{\text{lowcld}}(\vec{r}) = \sum_i \Theta_i(\vec{r})\Delta x_i(\vec{r}), \tag{5}$$

where $\Delta x_i(\vec{r})$ are the anomalies in each CCF $x_i(\vec{r})$, and $\Theta_i(\vec{r}) = \partial R^{\text{lowcld}}(\vec{r})/\partial x_i(\vec{r})$ are the radiative sensitivities to the CCFs (Ceppi et al., 2024; Myers et al., 2021; Scott et al., 2020). We apply CG19's refined energy budget model to understand inter-model differences in the contribution of SST patterns to variations in low cloud radiative anomaly across the historical time period. We incorporate the CG19 framework by decomposing the atmospheric variables used for CCF analysis as a combined response to a uniform warming and the SST pattern, such that the change in $R^{\text{lowcld}}(\vec{r})$ is approximated by

$$\Delta\tilde{R}^{\text{lowcld}}(\vec{r}) = \sum_i \Theta_i(\vec{r})\left(\frac{\partial x_i(\vec{r})}{\partial T_{\text{unif}}}\Delta T + \frac{\partial x_i(\vec{r})}{\partial S_p}\Delta S_p\right), \tag{6}$$

and can be decomposed into cloud radiative anomalies due to uniform warming

$$\Delta\tilde{R}^{\text{lowcld}}_{\text{unif}}(\vec{r}) \approx \sum_i \Theta_i(\vec{r})\frac{\partial x_i(\vec{r})}{\partial T_{\text{unif}}}\Delta T \tag{7}$$

and due to the SST pattern

$$\Delta\tilde{R}^{\text{lowcld}}_{p}(\vec{r}) \approx \sum_i \Theta_i(\vec{r})\frac{\partial x_i(\vec{r})}{\partial S_p}\Delta S_p. \tag{8}$$

Details of the derivation can be found in Text S1 of Supporting Information S1. Using CG19's available data, we conduct a limited verification that changes in the CCFs can be decomposed into a uniform and patterned response and that changes in the CCFs due to uniform warming exhibit no state dependence for one CMIP3-era model in Text S4, S5 and Figures S4, S5 of Supporting Information S1.

We calculate the low cloud feedback $(\tilde{\lambda}^{\text{lowcld}})$ by regressing Equation 6 against T. The first term in the brackets is a constant when regressed against T, such that the time-variation is solely from evolution of dS_p/dT in the second term. The models have qualitatively similar changes in CCFs in response to an increase in S_p (Figure S6 in Supporting Information S1), such that model spread predominantly comes from model differences in Θ_i (Figure S3 in Supporting Information S1). As we are interested in the spread in $\tilde{R}^{\text{lowcld}}_p$ feedback, we calculate $\tilde{\lambda}^{\text{lowcld}}_p$ by regressing the pattern component against T. We calculate the pattern component using the actual CCFs after removing uniform warming

$$\Delta\tilde{R}^{\text{lowcld}}_{p}(\vec{r}) \approx \sum_i \Theta_i\Delta x_i(\vec{r}) - \frac{\partial x_i(\vec{r})}{\partial T_{\text{unif}}}\Delta T, \tag{9}$$

rather than regressing against S_p as in Equation 8; using Equation 8 makes no difference for most of the models, but reduces the performance for CanESM5 (Figure S7 in Supporting Information S1).

Over the ocean, the CCFs are the surface temperature (ts), the EIS, the horizontal advection of SST (SSTadv), the relative humidity at 700 hPa (RH_{700}), the near-surface wind speed (ws), and the vertical velocity at 700 hPa

19448007, 2025, 17, Downloaded from https://agupubs.onlinelibrary.wiley.com/doi/10.1029/2025GL117015 by Imperial College London, Wiley Online Library on [30/10/2026]. See the Terms and Conditions (https://onlinelibrary.wiley.com/terms-and-conditions) on Wiley Online Library for rules of use; OA articles are governed by the applicable Creative Commons License

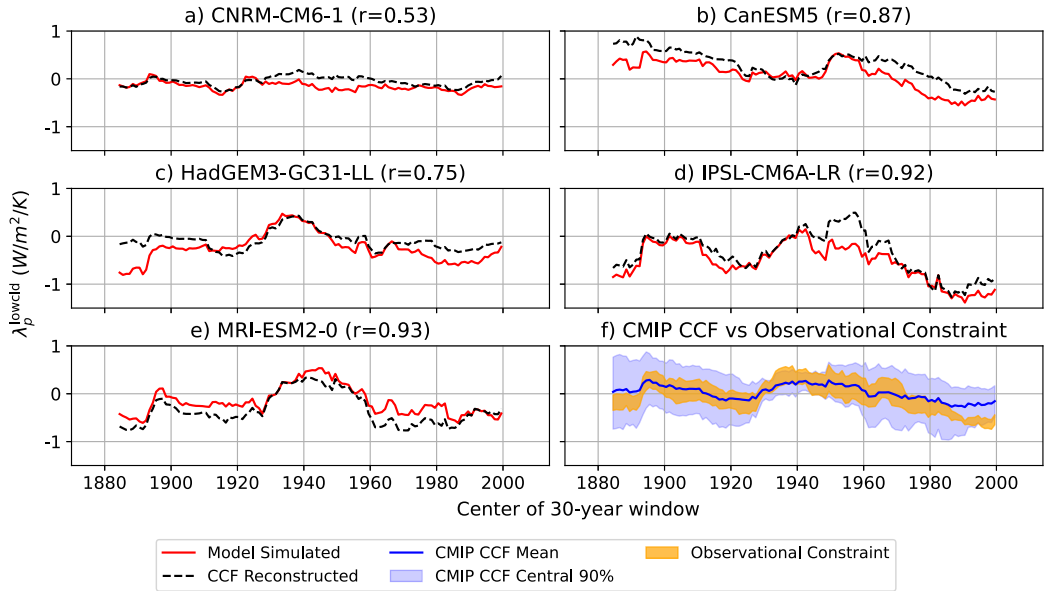


Figure 3. (a–e) The time-evolution across 30-year sliding windows of λ_p^{lowcld} from the *piForcing* run with the reconstructed $\tilde{\lambda}_p^{lowcld}$ from the models' cloud radiative sensitivities (CRSs) and cloud controlling factor (CCF) variations across sliding windows. (f) Comparison of the CMIP CCF-reconstructed $\tilde{\lambda}_p^{lowcld}$ with the observational constraint from MODIS across 30-year sliding windows. The blue shading is the central 90% of the CMIP calculated $\tilde{\lambda}_p^{lowcld}$ from the 16 CMIP CRSs convolved with the 6 sets of CCF changes from the *piForcing* runs, with the blue line being the mean. The orange shading is the observational constraint.

(ω_{700}) (Ceppi et al., 2024; Klein et al., 2017; Scott et al., 2020). Over land, SSTadv and ws are excluded, and EIS is replaced by the LTS (Ceppi et al., 2024; Ceppi & Nowack, 2021; Klein & Hartmann, 1993; Wood & Bretherton, 2006). We use the cloud radiative sensitivities (CRSs) (Θ_i in Equations 5–8) from Ceppi et al. (2024). They calculate CRSs from 16 CMIP5 and 6 models (see Table S1 in Supporting Information S1), and an observational CRS with cloud properties taken from the Moderate Resolution Imaging Spectroradiometer (MODIS) combined Aqua/Terra cloud property data set, collection 6.2, combined with CCFs calculated from the ERA5 reanalysis (Hersbach et al., 2020; MODIS Atmosphere Science Team, 2022; Pincus et al., 2023). Note that ERA5 is only used for calculating the observational CRS, and CCF changes in the observational constraint are from the same *piForcing* runs as the CMIP data.

4.2. CCFs Explain Time-Variation in Low Cloud Feedback

We verify that this approach is suitable for estimating the variations in low cloud feedbacks by calculating feedbacks across 30-year sliding windows. We calculate $\tilde{\lambda}_p^{lowcld}$ for the five models in which we also have the model-simulated λ_p^{lowcld}, and find that the CCF framework is able to replicate the model-simulated cloud feedback sufficiently well for assessing model spread (Figures 3a–3e). Thus, we are able to assess the time-evolution of cloud feedback across 16 CMIP-derived CRSs and the MODIS CRS by convolving the CRSs with the CCFs from each *piForcing* run. We find that the model-mean $\tilde{\lambda}_p^{lowcld}$ tends to underestimate the time-variance in the observationally constrained $\tilde{\lambda}_p^{lowcld}$ (Figure 3f). There is also substantial model spread in the time-series of the $\tilde{\lambda}_p^{lowcld}$. Notably, the observational constraint diverges from the CMIP central range in the period after 1980, *even when forced by the same CCF changes*. We obtain similar results if the CRSs are calculated from *amip* simulations instead of coupled historical simulations (Figure S8 in Supporting Information S1), so the model bias remains even if the CRSs are calculated from the observed warming pattern of the late 20th century.

We investigate this divergence by examining the last 30-year window including the years 1985–2014 (Figure 4). Only one model (IPSL-CM6A-LR) is able to replicate the strong negative observed $\tilde{\lambda}_p^{lowcld}$. However, it does this

19448007, 2025, 17, Downloaded from https://agupubs.onlinelibrary.wiley.com/doi/10.1029/2025GL117015 by Imperial College London, Wiley Online Library on [30/10/2026]. See the Terms and Conditions (https://onlinelibrary.wiley.com/terms-and-conditions) on Wiley Online Library for rules of use; OA articles are governed by the applicable Creative Commons License

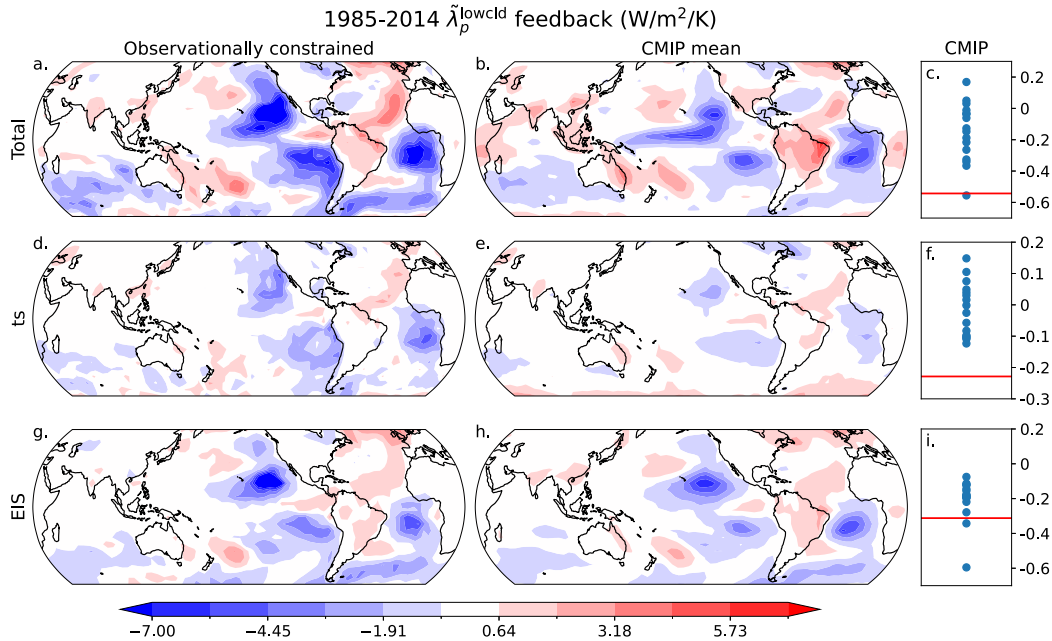


Figure 4. Comparison of the $\tilde{\lambda}_p^{\text{lowcld}}$ from convolving mean cloud controlling factor changes from 6 *piForcing* runs between 1980 and 2014. (a) the total feedback from the observational constraint, (b) the CMIP mean feedback and (c) area-averaged CMIP feedback, with the observational constraint as a red line. (d–f) the same as a-c, except for the feedback due to changes in ts. Panels (g–i) the same as panels (a–c), except for the feedback due to changes in estimated inversion strength.

for the wrong reasons, simulating an EIS response that is too strong (Figure 4i). The cause of the divergence between models and observations comes from all models underestimating the radiative response to local ts anomalies and most models underestimating the radiative response to EIS anomalies in the stratocumulus regions (Figures 4d–4i; Ceppi et al., 2024). The reason this discrepancy between observations and models does not occur at other times in the historical period is because the warming is more uniform (Andrews et al., 2022), meaning the contribution of local ts anomalies to $\lambda_p^{\text{lowcld}}$ is small; indeed, the only other period when the ts contribution was more negative than -0.15 W/m^2/K is the start of the *piForcing* period, the only other time when the CMIP CCF mean is not contained within the observational constraint (Figure S9 in Supporting Information S1).

We further investigate the model spread of $\tilde{R}_p^{\text{lowcld}}$ by calculating the $\tilde{R}_p^{\text{lowcld}}$ response to S_p $\left(d\tilde{R}_p^{\text{lowcld}}/dS_p\right)$ across the whole time-period for each model-derived CRS and the CCF changes from each *piForcing* run (Figure 5a). The spread from different radiative sensitivities (Θ_i) is greater than the spread from differing *piForcing* dynamical responses, consistent with the sensitivity analysis in Figure S3 of Supporting Information S1. We find that $d\tilde{R}_p^{\text{lowcld}}/dS_p$ inferred from the model-derived CRSs mostly underestimates the feedback inferred from MODIS, although GFDL-CM4, HadGEM2-ES and MRI-ESM2-0 are within the observational constraint depending on which *piForcing* run is used for the CCF changes, while IPSL-CM6A-LR overestimates $d\tilde{R}_p^{\text{lowcld}}/dS_p$. The observational constraint of $d\tilde{R}_p^{\text{lowcld}}/dS_p$ is -2.13 W/m^2/K (where the range from convolving with differing *piForcing* runs is $[-2.37,\ -1.98]$ W/m^2/K), while the CMIP CRS mean is -1.30 W/m^2/K (the central 66% is contained in the range $[-1.99,\ -0.68]$ W/m^2/K). Model-derived CRSs consistently underestimate the sensitivity to localized changes in ts (Figure 5b). However, the main driver of differences in $d\tilde{R}_p^{\text{lowcld}}/dS_p$ is the response to EIS anomalies ($r = 0.83$), particularly in the stratocumulus regions off the west coast of the Americas (Figure 5c). Similar to previous CCF analyses that looked at overall (rather than just patterned) changes relative to T (Ceppi et al., 2024; Myers et al., 2021; Scott et al., 2020), the global effect of CCFs other than ts and EIS is small, although the models simulate opposing SSTadv and RH700 responses which does not occur in the observational constraint. When comparing the locations that are most sensitive to changes in S_p, the models tend to simulate a strong cloud radiative response in the stratocumulus regions and the Equatorial Pacific. However,

19448007, 2025, 17, Downloaded from https://agupubs.onlinelibrary.wiley.com/doi/10.1029/2025GL117015 by Imperial College London, Wiley Online Library on [30/10/2026]. See the Terms and Conditions (https://onlinelibrary.wiley.com/terms-and-conditions) on Wiley Online Library for rules of use; OA articles are governed by the applicable Creative Commons License

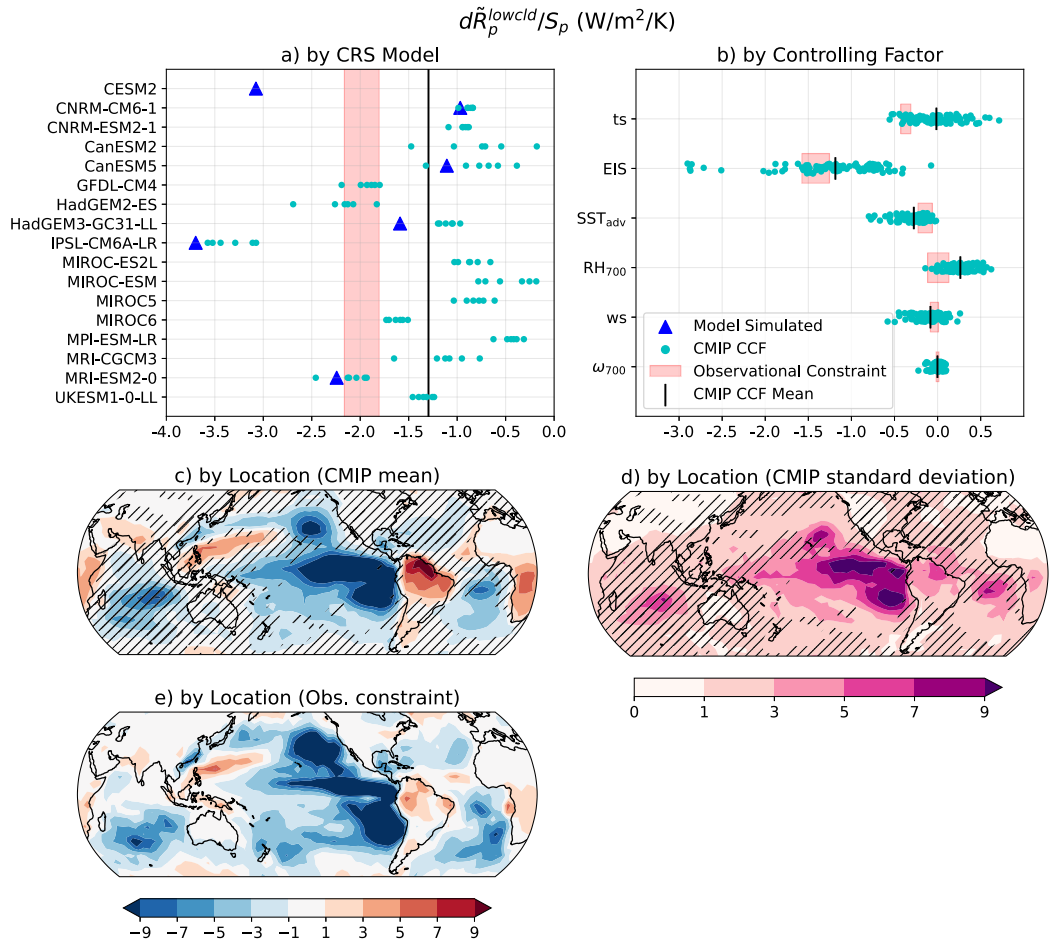


Figure 5. (a) $d\tilde{R}_p^{\text{lowcld}}/dS_p$ inferred from the different model-derived cloud radiative sensitivities (CRSs). In panels (a, b), each cyan dot is the model-derived kernel convolved with a different *piForcing* run. The blue triangles are $dR_p^{\text{lowcld}}/dS_p$ simulated by each model's *piForcing* run. The shaded red region is the $d\tilde{R}_p^{\text{lowcld}}/dS_p$ range obtained by convolving the MODIS-derived CRS with the *piForcing* runs. The black line is the mean value from the CMIP CRSs. CESM2 does not have a CRS, but has a *piForcing* run, so only has a blue triangle. (b) Contributions of individual CCFs to $d\tilde{R}_p^{\text{lowcld}}/dS_p$. (c) The mean $d\tilde{R}_p^{\text{lowcld}}/dS_p$ inferred from the model-derived CRSs by location. (d) The standard deviation of $d\tilde{R}_p^{\text{lowcld}}/dS_p$ inferred from the model-derived CRSs by location. The standard deviations are calculated based on $d\tilde{R}_p^{\text{lowcld}}/dS_p$ from each model's CRSs combined with the mean cloud controlling factor (CCF) changes of the *piForcing* runs. In panels (c, d), stippling shows regions where the mean is within one standard deviation of 0. (e) The $d\tilde{R}_p^{\text{lowcld}}/dS_p$ inferred from the observational constraint by location. The observational constraint is calculated with the mean CCF changes of the *piForcing* runs.

these regions also have the greatest model variance, particularly off the western coast of South America (Figure 5d). Compared to the observational constraint, the models are largely able to capture the correct spatial distribution, although they underestimate the negative feedback in the Northeast Pacific and simulate too strong a positive feedback over land areas (Figure 5e).

5. Discussion and Conclusions

Evolving patterns of SST are known to affect Earth's radiative feedbacks on decadal time scales (Gregory & Andrews, 2016; Zhou et al., 2016). For example, in recent decades, a strong zonal SST gradient in the equatorial Pacific has promoted an increase in atmospheric stability, increasing low clouds in tropical subsidence regions (Andrews & Webb, 2018; Ceppi & Gregory, 2017; Zhou et al., 2016). Past work examining the historical pattern effect has determined that climate feedbacks have been more stabilizing than those expected from abrupt

19448007, 2025, 17, Downloaded from https://agupubs.onlinelibrary.wiley.com/doi/10.1029/2025GL117015 by Imperial College London, Wiley Online Library on [30/10/2026]. See the Terms and Conditions (https://onlinelibrary.wiley.com/terms-and-conditions) on Wiley Online Library for rules of use; OA articles are governed by the applicable Creative Commons License

19448007, 2025, 17, Downloaded from https://agupubs.onlinelibrary.wiley.com/doi/10.1029/2025GL117015 by Imperial College London, Wiley Online Library on [30/10/2026]. See the Terms and Conditions (https://onlinelibrary.wiley.com/terms-and-conditions) on Wiley Online Library for rules of use; OA articles are governed by the applicable Creative Commons License

increases in CO_2 (Andrews et al., 2018, 2022; Gregory & Andrews, 2016; Zhou et al., 2016). The cloud radiative response to evolving SST patterns, particularly the component due to low clouds, is the primary driver of this variation (Andrews et al., 2022; Myers et al., 2023). However, there has been limited work that examined the regions and cloud types which caused differences in the representation of the historical pattern effect between different atmospheric models.

This study analyzed model output from 6 atmospheric models from the CMIP6 generation forced by observed SST and sea ice concentrations (*piForcing* experiments) for the time period 1870–2014. We showed model spread in time-variation of the climate feedback was dominated by differences in the radiative sensitivity of low clouds to changes in LTS. We then applied CCF analysis (Ceppi et al., 2024; Klein et al., 2017) to the refined energy budget of Ceppi and Gregory (2019) to further analyze model differences in cloud radiative sensitivity for sensitivity coefficients derived from 16 CMIP5/6 models in the low cloud response to the SST pattern. We identified that the variance of the low cloud feedback time-variation among climate models is largely caused by the spread in radiative sensitivity to EIS, and that most models tend to underestimate this sensitivity (Figure 5). While the finding that model spread in time-variation is because of EIS radiative sensitivity is a novel result, it is not particularly surprising. It was known that low cloud radiative sensitivity to changes in surface temperature is the primary driver of model differences in the long-term low cloud feedback (Ceppi & Nowack, 2021; Myers et al., 2021; Myers & Norris, 2016; Qu et al., 2014), and from previous CCF analyses that EIS variation was the driver of decadal variations in the low cloud feedback (Myers et al., 2023).

Additionally, we found that the pattern of warming after 1980 accentuated known model underestimations of cloud feedbacks to localized temperature changes in the stratocumulus regions(Ceppi et al., 2024), resulting in a divergence between $\tilde{\lambda}_p^{\text{lowcld}}$ predicted by the CMIP Θs and the observational constraint, even when driven by the same CCF changes (Figure 4). Our observational constraint derived from MODIS finds that the most recent period has the most negative cloud feedback, consistent with Myers et al. (2023), who applied the radiative sensitivities from Scott et al. (2020) to CCF changes from *piForcing*.

By focusing on the historical SST pattern effect, we have not considered how the variation in low cloud sensitivity feeds back on the SST pattern itself. Recent work has shown the importance of cloud feedbacks in shaping the zonal gradient across the tropical Pacific (Breul et al., 2025; Espinosa & Zelinka, 2024; Hsiao et al., 2022). Our work suggests the importance of the cloud response to S_p as a key source of model spread in the time-variation of low cloud feedbacks. However, our findings also highlight the importance of models underestimating the cloud radiative response to localized SST changes as a driver of multi-model bias (Figures 4 and 5; Ceppi et al., 2024; Espinosa & Zelinka, 2024). Further investigation of how the differing strengths of the surface temperature and lower-tropospheric stability feedbacks affect the SST pattern is needed.

Data Availability Statement

All data sets used here are freely available online. Data from CMIP5 (Taylor et al., 2012) and CMIP6 (Eyring et al., 2016) were downloaded from the Earth System Grid Federation (Cinquini et al., 2014), accessible at https://aims2.llnl.gov/search. Cloud radiative kernels were downloaded from Zelinka (2021). The observational cloud-radiative sensitivities were calculated from MODIS satellite observations (MODIS Atmosphere Science Team, 2022) and ERA5 reanalysis data (Copernicus Climate Change Service, 2019a, 2019b).

Acknowledgments
The authors thank Tim Andrews and an anonymous reviewer for their comments which greatly improved this manuscript. KK was supported through the UK Natural Environment Research Council Grant NE/S007415/1. PC was supported by UK Research and Innovation (UKRI) under the UK government's Horizon Europe funding Guarantee (Grant EP/Y036123/1), and through UK Natural Environmental Research Council Grants NE/V012045/1 and NE/T006250/1.

References

Andrews, T., Bodas-Salcedo, A., Gregory, J. M., Dong, Y., Armour, K. C., Paynter, D., et al. (2022). On the effect of historical SST patterns on radiative feedback. *Journal of Geophysical Research: Atmospheres*, *127*(18), e2022JD036675. https://doi.org/10.1029/2022JD036675

Andrews, T., Gregory, J. M., Paynter, D., Silvers, L. G., Zhou, C., Mauritsen, T., et al. (2018). Accounting for changing temperature patterns increases historical estimates of climate sensitivity. *Geophysical Research Letters*, *45*(16), 8490–8499. https://doi.org/10.1029/2018GL078887

Andrews, T., Gregory, J. M., & Webb, M. J. (2015). The dependence of radiative forcing and feedback on evolving patterns of surface temperature change in climate models. *Journal of Climate*, *28*(4), 1630–1648. https://doi.org/10.1175/JCLI-D-14-00545.1

Andrews, T., & Webb, M. J. (2018). The dependence of global cloud and lapse rate feedbacks on the spatial structure of tropical pacific warming. *Journal of Climate*, *31*(2), 641–654. https://doi.org/10.1175/JCLI-D-17-0087.1

Bodas-Salcedo, A., Webb, M. J., Bony, S., Chepfer, H., Dufresne, J.-L., Klein, S. A., et al. (2011). COSP: Satellite simulation software for model assessment. *Bulletin of the American Meteorological Society*, *92*(8), 1023–1043. https://doi.org/10.1175/2011BAMS2856.1

Bony, S., & Dufresne, J.-L. (2005). Marine boundary layer clouds at the heart of tropical cloud feedback uncertainties in climate models. *Geophysical Research Letters*, *32*(20), 2005GL023851. https://doi.org/10.1029/2005GL023851

Breul, P., Ceppi, P., & Nowack, P. (2025). The importance of stratocumulus clouds for projected warming patterns and circulation changes. *EGUsphere*. (preprint). https://doi.org/10.5194/egusphere-2025-221

Ceppi, P., Brient, F., Zelinka, M. D., & Hartmann, D. L. (2017). Cloud feedback mechanisms and their representation in global climate models. *WIREs Climate Change*, *8*(4), e465. https://doi.org/10.1002/wcc.465

Ceppi, P., & Fueglistaler, S. (2021). The El Niño–Southern Oscillation pattern effect. *Geophysical Research Letters*, *48*(21), e2021GL095261. https://doi.org/10.1029/2021GL095261

Ceppi, P., & Gregory, J. M. (2017). Relationship of tropospheric stability to climate sensitivity and Earth's observed radiation budget. *Proceedings of the National Academy of Sciences* (Vol. 114(50), pp. 13126–13131). https://doi.org/10.1073/pnas.1714308114

Ceppi, P., & Gregory, J. M. (2019). A refined model for the Earth's global energy balance. *Climate Dynamics*, *53*(7–8), 4781–4797. https://doi.org/10.1007/s00382-019-04825-x

Ceppi, P., Myers, T. A., Nowack, P., Wall, C. J., & Zelinka, M. D. (2024). Implications of a pervasive climate model bias for low-cloud feedback. *Geophysical Research Letters*, *51*(20), e2024GL110525. https://doi.org/10.1029/2024GL110525

Ceppi, P., & Nowack, P. (2021). Observational evidence that cloud feedback amplifies global warming. *Proceedings of the National Academy of Sciences* (Vol. 118(30), e2026290118). https://doi.org/10.1073/pnas.2026290118

Chao, L.-W., Muller, J. C., & Dessler, A. E. (2022). Impacts of the unforced pattern effect on the cloud feedback in CERES observations and climate models. *Geophysical Research Letters*, *49*(2), e2021GL096299. https://doi.org/10.1029/2021GL096299

Cinquini, L., Crichton, D., Mattmann, C., Harney, J., Shipman, G., Wang, F., et al. (2014). The Earth System Grid Federation: An open infrastructure for access to distributed geospatial data. *Future Generation Computer Systems*, *36*, 400–417. https://doi.org/10.1016/j.future.2013.07.002

Copernicus Climate Change Service. (2019a). ERA5 monthly averaged data on pressure levels from 1940 to present [Dataset]. *Copernicus Climate Change Service (C3S) Climate Data Store (CDS)*. https://doi.org/10.24381/CDS.6860A573

Copernicus Climate Change Service. (2019b). ERA5 monthly averaged data on single levels from 1940 to present [Dataset]. *Copernicus Climate Change Service (C3S) Climate Data Store (CDS)*. https://doi.org/10.24381/CDS.F17050D7

Dong, Y., Armour, K. C., Zelinka, M. D., Proistosescu, C., Battisti, D. S., Zhou, C., & Andrews, T. (2020). Intermodel spread in the pattern effect and its contribution to climate sensitivity in CMIP5 and CMIP6 models. *Journal of Climate*, *33*(18), 7755–7775. https://doi.org/10.1175/JCLI-D-19-1011.1

Dong, Y., Proistosescu, C., Armour, K. C., & Battisti, D. S. (2019). Attributing historical and future evolution of radiative feedbacks to regional warming patterns using a green's function approach: The preeminence of the Western Pacific. *Journal of Climate*, *32*(17), 5471–5491. https://doi.org/10.1175/JCLI-D-18-0843.1

Eiselt, K.-U., & Graversen, R. G. (2022). Change in climate sensitivity and its dependence on the lapse-rate feedback in $4 \times CO_2$ climate model experiments. *Journal of Climate*, *35*(9), 2919–2932. https://doi.org/10.1175/JCLI-D-21-0623.1

Espinosa, Z. I., & Zelinka, M. D. (2024). The shortwave cloud-SST feedback amplifies multi-decadal Pacific sea surface temperature trends: Implications for observed cooling. *Geophysical Research Letters*, *51*(18), e2024GL111039. https://doi.org/10.1029/2024GL111039

Eyring, V., Bony, S., Meehl, G. A., Senior, C. A., Stevens, B., Stouffer, R. J., & Taylor, K. E. (2016). Overview of the Coupled Model Intercomparison Project Phase 6 (CMIP6) experimental design and organization. *Geoscientific Model Development*, *9*(5), 1937–1958. https://doi.org/10.5194/gmd-9-1937-2016

Gregory, J. M., & Andrews, T. (2016). Variation in climate sensitivity and feedback parameters during the historical period. *Geophysical Research Letters*, *43*(8), 3911–3920. https://doi.org/10.1002/2016GL068406

Gregory, J. M., Andrews, T., Ceppi, P., Mauritsen, T., & Webb, M. J. (2020). How accurately can the climate sensitivity to CO_2 be estimated from historical climate change? *Climate Dynamics*, *54*(1–2), 129–157. https://doi.org/10.1007/s00382-019-04991-y

Gregory, J. M., Ingram, W. J., Palmer, M. A., Jones, G. S., Stott, P. A., Thorpe, R. B., et al. (2004). A new method for diagnosing radiative forcing and climate sensitivity. *Geophysical Research Letters*, *31*(3), 2003GL018747. https://doi.org/10.1029/2003GL018747

Haugstad, A. D., Armour, K. C., Battisti, D. S., & Rose, B. E. J. (2017). Relative roles of surface temperature and climate forcing patterns in the inconstancy of radiative feedbacks. *Geophysical Research Letters*, *44*(14), 7455–7463. https://doi.org/10.1002/2017GL074372

He, H., Kramer, R. J., & Soden, B. J. (2021). Evaluating observational constraints on intermodel spread in cloud, temperature, and humidity feedbacks. *Geophysical Research Letters*, *48*(17), e2020GL092309. https://doi.org/10.1029/2020GL092309

Hersbach, H., Bell, B., Berrisford, P., Hirahara, S., Horányi, A., Muñoz-Sabater, J., et al. (2020). The ERA5 global reanalysis. *Quarterly Journal of the Royal Meteorological Society*, *146*(730), 1999–2049. https://doi.org/10.1002/qj.3803

Hsiao, W.-T., Hwang, Y.-T., Chen, Y.-J., & Kang, S. M. (2022). The role of clouds in shaping tropical Pacific response pattern to extratropical thermal forcing. *Geophysical Research Letters*, *49*(11), e2022GL098023. https://doi.org/10.1029/2022GL098023

Hurrell, J. W., Hack, J. J., Shea, D., Caron, J. M., & Rosinski, J. (2008). A new sea surface temperature and sea ice boundary dataset for the community atmosphere model. *Journal of Climate*, *21*(19), 5145–5153. https://doi.org/10.1175/2008JCLI2292.1

Klein, S. A., Hall, A., Norris, J. R., & Pincus, R. (2017). Low-cloud feedbacks from cloud-controlling factors: A review. *Surveys in Geophysics*, *38*(6), 1307–1329. https://doi.org/10.1007/s10712-017-9433-3

Klein, S. A., & Hartmann, D. L. (1993). The seasonal cycle of low stratiform clouds. *Journal of Climate*, *6*(8), 1587–1606. https://doi.org/10.1175/1520-0442(1993)006⟨1587:TSCOLS⟩2.0.CO;2

Marvel, K., Pincus, R., Schmidt, G. A., & Miller, R. L. (2018). Internal variability and disequilibrium confound estimates of climate sensitivity from observations. *Geophysical Research Letters*, *45*(3), 1595–1601. https://doi.org/10.1002/2017GL076468

MODIS Atmosphere Science Team. (2022). MODIS (Aqua/Terra) cloud properties level 3 monthly, 1×1 degree grid [Dataset]. *NASA Level 1 and Atmosphere Archive and Distribution System Distributed Active Archive Center*. https://doi.org/10.5067/MODIS/MCD06COSP_M3_MODIS.062

Myers, T. A., & Norris, J. R. (2016). Reducing the uncertainty in subtropical cloud feedback. *Geophysical Research Letters*, *43*(5), 2144–2148. https://doi.org/10.1002/2015GL067416

Myers, T. A., Scott, R. C., Zelinka, M. D., Klein, S. A., Norris, J. R., & Caldwell, P. M. (2021). Observational constraints on low cloud feedback reduce uncertainty of climate sensitivity. *Nature Climate Change*, *11*(6), 501–507. https://doi.org/10.1038/s41558-021-01039-0

Myers, T. A., Zelinka, M. D., & Klein, S. A. (2023). Observational constraints on the cloud feedback pattern effect. *Journal of Climate*, *36*(18), 6533–6545. https://doi.org/10.1175/JCLI-D-22-0862.1

Pincus, R., Hubanks, P. A., Platnick, S., Meyer, K., Holz, R. E., Botambekov, D., & Wall, C. J. (2023). Updated observations of clouds by MODIS for global model assessment. *Earth System Science Data*, *15*(6), 2483–2497. https://doi.org/10.5194/essd-15-2483-2023

Qu, X., Hall, A., Klein, S. A., & Caldwell, P. M. (2014). On the spread of changes in marine low cloud cover in climate model simulations of the 21st century. *Climate Dynamics*, *42*(9–10), 2603–2626. https://doi.org/10.1007/s00382-013-1945-z

19448007, 2025, 17, Downloaded from https://agupubs.onlinelibrary.wiley.com/doi/10.1029/2025GL117015 by Imperial College London, Wiley Online Library on [30/10/2026]. See the Terms and Conditions (https://onlinelibrary.wiley.com/terms-and-conditions) on Wiley Online Library for rules of use; OA articles are governed by the applicable Creative Commons License

Ringer, M. A., Andrews, T., & Webb, M. J. (2014). Global-mean radiative feedbacks and forcing in atmosphere-only and coupled atmosphere-ocean climate change experiments. *Geophysical Research Letters*, *41*(11), 4035–4042. https://doi.org/10.1002/2014GL060347

Ringer, M. A., Bodas-Salcedo, A., & Webb, M. J. (2023). Global and regional climate feedbacks in response to uniform warming and cooling. *Journal of Geophysical Research: Atmospheres*, *128*(24), e2023JD038861. https://doi.org/10.1029/2023JD038861

Scott, R. C., Myers, T. A., Norris, J. R., Zelinka, M. D., Klein, S. A., Sun, M., & Doelling, D. R. (2020). Observed sensitivity of low-cloud radiative effects to meteorological perturbations over the global oceans. *Journal of Climate*, *33*(18), 7717–7734. https://doi.org/10.1175/JCLI-D-19-1028.1

Sherwood, S. C., Bony, S., Boucher, O., Bretherton, C., Forster, P. M., Gregory, J. M., & Stevens, B. (2015). Adjustments in the forcing-feedback framework for understanding climate change. *Bulletin of the American Meteorological Society*, *96*(2), 217–228. https://doi.org/10.1175/BAMS-D-13-00167.1

Sherwood, S. C., Webb, M. J., Annan, J. D., Armour, K. C., Forster, P. M., Hargreaves, J. C., et al. (2020). An assessment of Earth's climate sensitivity using multiple lines of evidence. *Reviews of Geophysics*, *58*(4), e2019RG000678. https://doi.org/10.1029/2019RG000678

Silvers, L. G., Paynter, D., & Zhao, M. (2018). The diversity of cloud responses to twentieth century sea surface temperatures. *Geophysical Research Letters*, *45*(1), 391–400. https://doi.org/10.1002/2017GL075583

Stevens, B., & Brenguier, J.-L. (2009). Cloud-controlling factors. In J. Heintzenberg & R. J. Charlson (Eds.), *Clouds in the perturbed climate System* (pp. 173–196). The MIT Press. https://doi.org/10.7551/mitpress/9780262012874.003.0008

Stevens, B., Sherwood, S. C., Bony, S., & Webb, M. J. (2016). Prospects for narrowing bounds on Earth's equilibrium climate sensitivity. *Earth's Future*, *4*(11), 512–522. https://doi.org/10.1002/2016EF000376

Taylor, K. E., Stouffer, R. J., & Meehl, G. A. (2012). An overview of CMIP5 and the experiment design. *Bulletin of the American Meteorological Society*, *93*(4), 485–498. https://doi.org/10.1175/BAMS-D-11-00094.1

Webb, M. J., Andrews, T., Bodas-Salcedo, A., Bony, S., Bretherton, C. S., Chadwick, R., et al. (2017). The Cloud Feedback Model Intercomparison Project (CFMIP) contribution to CMIP6. *Geoscientific Model Development*, *10*(1), 359–384. https://doi.org/10.5194/gmd-10-359-2017

Williams, A. I. L., Jeevanjee, N., & Bloch-Johnson, J. (2023). Circus tents, convective thresholds, and the non-linear climate response to tropical SSTs. *Geophysical Research Letters*, *50*(6), e2022GL101499. https://doi.org/10.1029/2022GL101499

Wood, R., & Bretherton, C. S. (2006). On the relationship between stratiform low cloud cover and lower-tropospheric stability. *Journal of Climate*, *19*(24), 6425–6432. https://doi.org/10.1175/JCLI3988.1

Zelinka, M. (2021). Mzelinka/cloud-radiative-kernels: Sep 17, 2021 release [Software]. *Zenodo*. https://doi.org/10.5281/ZENODO.5514137

Zelinka, M. D., Chao, L.-W., Myers, T. A., Qin, Y., & Klein, S. A. (2025). Technical note: Recommendations for diagnosing cloud feedbacks and rapid cloud adjustments using cloud radiative kernels. *Atmospheric Chemistry and Physics*, *25*(3), 1477–1495. https://doi.org/10.5194/acp-25-1477-2025

Zelinka, M. D., Klein, S. A., & Hartmann, D. L. (2012). Computing and partitioning cloud feedbacks using cloud property histograms. Part I: Cloud radiative Kernels. *Journal of Climate*, *25*(11), 3715–3735. https://doi.org/10.1175/JCLI-D-11-00248.1

Zelinka, M. D., Myers, T. A., McCoy, D. T., Po-Chedley, S., Caldwell, P. M., Ceppi, P., et al. (2020). Causes of higher climate sensitivity in CMIP6 models. *Geophysical Research Letters*, *47*(1), e2019GL085782. https://doi.org/10.1029/2019GL085782

Zhou, C., Zelinka, M. D., & Klein, S. A. (2016). Impact of decadal cloud variations on the Earth's energy budget. *Nature Geoscience*, *9*(12), 871–874. https://doi.org/10.1038/ngeo2828

Zhou, C., Zelinka, M. D., & Klein, S. A. (2017). Analyzing the dependence of global cloud feedback on the spatial pattern of sea surface temperature change with a Green's function approach. *Journal of Advances in Modeling Earth Systems*, *9*(5), 2174–2189. https://doi.org/10.1002/2017MS001096

References From the Supporting Information

Bloch-Johnson, J., Pierrehumbert, R. T., & Abbot, D. S. (2015). Feedback temperature dependence determines the risk of high warming. *Geophysical Research Letters*, *42*(12), 4973–4980. https://doi.org/10.1002/2015GL064240

Bloch-Johnson, J., Rugenstein, M., Stolpe, M. B., Rohrschneider, T., Zheng, Y., & Gregory, J. M. (2021). Climate sensitivity increases under higher CO_2 levels due to feedback temperature dependence. *Geophysical Research Letters*, *48*(4), e2020GL089074. https://doi.org/10.1029/2020GL089074

Caldwell, P. M., Zelinka, M. D., Taylor, K. E., & Marvel, K. (2016). Quantifying the sources of intermodel spread in equilibrium climate sensitivity. *Journal of Climate*, *29*(2), 513–524. https://doi.org/10.1175/JCLI-D-15-0352.1

Held, I. M., & Shell, K. M. (2012). Using relative humidity as a state variable in climate feedback analysis. *Journal of Climate*, *25*(8), 2578–2582. https://doi.org/10.1175/JCLI-D-11-00721.1

Janoski, T. P., Mitevski, I., Kramer, R. J., Previdi, M., & Polvani, L. M. (2025). ClimKern v1.2: A new Python package and kernel repository for calculating radiative feedbacks. *Geoscientific Model Development*, *18*(10), 3065–3079. https://doi.org/10.5194/gmd-18-3065-2025

Soden, B. J., & Held, I. M. (2006). An assessment of climate feedbacks in coupled ocean–atmosphere models. *Journal of Climate*, *19*(14), 3354–3360. https://doi.org/10.1175/JCLI3799.1

Soden, B. J., Held, I. M., Colman, R., Shell, K. M., Kiehl, J. T., & Shields, C. A. (2008). Quantifying climate feedbacks using radiative Kernels. *Journal of Climate*, *21*(14), 3504–3520. https://doi.org/10.1175/2007JCLI2110.1

Zelinka, M. D., Zhou, C., & Klein, S. A. (2016). Insights from a refined decomposition of cloud feedbacks. *Geophysical Research Letters*, *43*(17), 9259–9269. https://doi.org/10.1002/2016GL069917

Zhou, C., Wang, M., Zelinka, M. D., Liu, Y., Dong, Y., & Armour, K. C. (2023). Explaining forcing efficacy with pattern effect and state dependence. *Geophysical Research Letters*, *50*(3), e2022GL101700. https://doi.org/10.1029/2022GL101700

19448007, 2025, 17, Downloaded from https://agupubs.onlinelibrary.wiley.com/doi/10.1029/2025GL117015 by Imperial College London, Wiley Online Library on [30/10/2026]. See the Terms and Conditions (https://onlinelibrary.wiley.com/terms-and-conditions) on Wiley Online Library for rules of use; OA articles are governed by the applicable Creative Commons License